solution obtained within a few seconds was layered with a mixture of 2-propanol and *n*-heptane (1:1 v/v, 80 mL). When the diffusion was completed, brown-red crystals of the product were recovered as in part 1, with yields of ca. 75%.

5. Synthesis of [PPN][$Rh_5(CO)_{14}(PPh_3)$]. (a) From [PPN][$Rh_5(CO)_{15}$] and PPh_3. [PPN][$Rh_5(CO)_{15}$] (0.265 g, 0.180 mmol) in THF (2.2 mL), under CO, was treated while being stirred, with PPh_3 (0.052 g, 0.198 mmol, 1.1:1). An immediate reaction was observed with CO evolution and change of the color to orange, while the IR spectrum showed quantitative formation of the $[Rh_5(CO)_{14}(PPh_3)]^-$ anion. After 1 h, the solution was cautiously layered with a mixture of 2-propanol (16 mL) and *n*-hexane (8 mL) previously saturated with CO. The product separated out initially as an oil, which eventually slowly crystallized almost completely. When the diffusion of the solvents was completed (ca. 1 week), the mother liquor was syringed off and the mixture of crystals and solidified oil was washed with 2-propanol (6 mL), then briefly vacuum-dried, and stored under CO. Both the crystals and the amorphous solid have the same IR spectrum. Though the reaction appears quantitative, some product is lost in the mother liquor, to give final yields of ca. 80-85%.

(b) By Replacement of X^- on $[PPN]_2[Rh_5(CO)_{14}X]$ (X = I, Br). A red-orange solution of $[PPN]_2[Rh_5(CO)_{14}I]$ or $[PPh_4]_2[Rh_5(CO)_{14}Br]$ (0.05 g) in THF (3 mL) under CO, was treated, while being stirred, with a slight excess of PPh_3. Immediate reaction was observed, with formation of a white precipitate and color change to orange-yellow, while the IR spectrum showed that the absorptions of the starting anions were completely replaced by those of $[Rh_5(CO)_{14}(PPh_3)]^-$. The white precipitate was recognized as [PPN]I or $[PPh_4]Br$, respectively.

6. X-ray Analysis. Crystallographic data for both compounds are reported in Table III; details of the data collection are given in the supplementary material (Table S1). Both collections were performed with crystal samples sealed under nitrogen atmosphere in a Lindemann capillary, and no decay was observed.

The structures were solved by Patterson and Fourier methods and refined by full-matrix least-squares techniques. In both cases, the metal, the phosphorus, and the sulfur atoms were refined with anisotropic thermal parameters. In the refinement of $[PPN]_2[Rh_5(CO)_{14}(SCN)]$ the phenyl rings were treated as rigid bodies of D_{6h} symmetry. The final conventional agreement factors $R = \sum(F_o - k|F_c|)/\sum F_o$ and $R_w = [\sum w(F_o - k|F_c|)^2/\sum wF_o^2]^{1/2}$ were, respectively, 0.041 and 0.050 in the PPh_3 derivative and 0.069 and 0.092 in the SCN derivative. Weights were assigned to individual observations according to the formula $w = 4F_o^2/\sigma(F_o^2)^2$, where $\sigma(F_o^2) = [\sigma(I)^2 + (pI)^2]^{1/2}/LP$ and p the "ignorance factor" is equal to 0.03. The computations were made, in the case of the PPh_3 derivative, on a PDP 11/34 computer using the Enraf-Nonius Structure Determination Package (SDP) and the physical constants therein tabulated; in the case of the SCN derivative an Univac 1100/80 computer was used with local programs.

The final positional parameters are reported in Tables IV and V.

Supplementary Material Available: Crystal data and details of the intensity measurements for both $[(Ph_3P)_2N][Rh_5(CO)_{14}PPh_3]$ (I) and $[(Ph_3P)_2N]_2[Rh_5(CO)_{14}SCN]$ (II) (Table S1) and thermal parameters for I and II (Table S2) (2 pages); two lists of computed and observed structure factor moduli (Table S3 for I and Table S4 for II) (57 pages). Ordering information is given on any current masthead page.

Contribution from the Department of Chemistry, North Carolina State University, Raleigh, North Carolina 27695-8204, and Laboratoire de Chimie des Solides, IPCM, Université de Nantes, 44072 Nantes Cedex 03, France

Structural Origin of the Electronic Instability in Titanium Bronze $Na_{0.25}TiO_2$

Michel Evain,[†] Myung-Hwan Whangbo,*[,†] Luc Brohan,[‡] and René Marchand[‡]

Received September 1, 1989

The origin of the charge density wave phenomenon in $Na_{0.25}TiO_2$ was investigated by examining the octahedral distortions in $Na_{0.25}TiO_2$ and by calculating the tight-binding band electronic structure of $Na_{0.25}TiO_2$. Despite its three-dimensional lattice, $Na_{0.25}TiO_2$ is essentially a one-dimensional metal. This finding is explained on the basis of the distortions present in the TiO_6 octahedra of the $Na_{0.25}TiO_2$ lattice.

Recently, Brohan et al have shown[1] that sodium titanium bronze $Na_{0.25}TiO_2$ undergoes a metal-insulator transition at 630 K. This phase transition is caused by a Peierls instability normally associated with one-dimensional (1D) metals, because $Na_{0.25}TiO_2$ shows incommensurate superlattice spots centered at (a^*, q_{b^*}, 0) below 430 K.[1,2] The q_{b^*} value of this charge density wave (CDW) is found to increase gradually from $0.230b^*$ at 430 K to $0.245b^*$ at room temperature. Such a temperature dependence of CDW superlattice spot positions has been observed in molybdenum blue bronze $A_{0.3}MoO_3$ (A = K, Rb, Tl),[3,4] which contains Mo-O layers made up of MoO_6 octahedra. Since these Mo-O layers are separated by the A atoms, blue bronze has a two-dimensional structural character. However, blue bronze is a 1D metal[5] because of the way the MoO_6 octahedra are distorted in each Mo-O layer.[6] Sodium titanium bronze $Na_{0.25}TiO_2$ has a three-dimensional (3D) Ti-O lattice made up of TiO_6 octahedra,[1a] so that a particular pattern of distortion must exist in the TiO_6 octahedra for the 3D Ti-O lattice to have a 1D metallic character. Thus it is important to understand how the electronic structure of $Na_{0.25}TiO_2$ is related to its crystal structure. The main objective of the present study is to examine this structure-property relationship. In the following, we first describe the crystal structure of $Na_{0.25}TiO_2$ from the viewpoint of TiO_6 octahedra and then analyze its tight-binding band electronic structure[7] calculated by the extended Hückel method.[8] The atomic parameters used in our study are summarized in Table I.

Table I. Exponents ζ_i and Valence Shell Ionization Potentials H_{ii} for Slater-Type Orbitals χ_i[a,b]

χ_i	ζ_i	ζ_i'	H_{ii}, eV
Ti 3d	4.55 (0.4206)	1.40 (0.7839)	-10.81
O 2s	2.275		-32.3
O 2p	2.275		-14.8

[a] The d orbitals of Ti are given as a linear combination of two Slater type orbitals, and each is followed by a weighting factor in parentheses. [b] A modified Wolfsberg-Helmholz formula was used to calculate H_{ij}.[10]

[†] North Carolina State University.
[‡] Université de Nantes.

(1) (a) Brohan, L. Ph.D. Thesis, Université Nantes, 1986. (b) Brohan, L.; Marchand, R.; Tournoux, M. *J. Solid State Chem.* **1988**, *72*, 145.
(2) Colaitis, D.; Coene, W.; Amelinckx, S.; Brohan, L.; Marchand, R. *J. Solid State Chem.* **1988**, *75*, 156.
(3) (a) Pouget, J. P.; Noguera, C.; Moudden, A. H.; Moret, T. *J. Phys.* (*Les Ulis, Fr.*) **1985**, *46*, 1731. (b) Pouget, J. P.; Kagoshima, S.; Schlenker, C.; Marcus, J. *J. Phys. Lett.* **1983**, *44*, 6133. (c) Fleming, R.; Schneemeyer, L. F.; Moncton, D. E. *Phys. Rev. B* **1988**, *31*, 899. (d) Tamegai, T.; Tsutsumi, K.; Kagoshima, S.; Kanai, Y.; Taui, M.; Tomozawa, H.; Sato, M.; Tsuji, K.; Harada, J.; Sakata, M.; Nakajima, T. *Solid State Commun.* **1984**, *51*, 585.
(4) (a) Ghedira, M.; Chenavas, J.; Marezio, M.; Marcus, J. *J. Solid State Chem.* **1985**, *57*, 300. (b) Ganne, M.; Boumaza, A.; Dion, M.; Dumas, J. *Mater. Res. Bull.* **1988**, *20*, 1297. (c) Graham, J.; Wadsley, A. D. *Acta Crystallogr.* **1966**, *20*, 93.
(5) Whangbo, M.-H.; Schneemeyer, L. F. *Inorg. Chem.* **1986**, *25*, 2424.

0020-1669/90/1329-1413$02.50/0

Crystal Structure

It is convenient to describe the crystal structure of $Na_{0.25}TiO_2$ in terms of a TiO_5 single chain **1** built from TiO_6 octahedra upon sharing their corners. A Ti_2O_8 double chain **2a** is obtained from

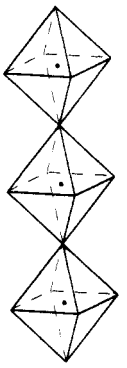

1

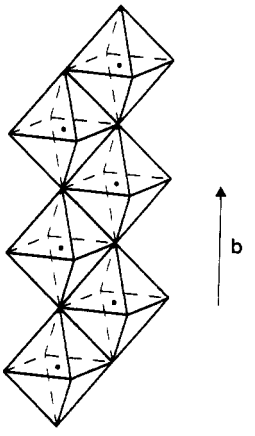

2a

two TiO_5 chains **1** by sharing their octahedral edges. **2b** represents

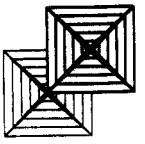

2b

a projection view of the Ti_2O_8 double chain **2a** along the chain direction. In terms of such a projection view, it is easy to build the 3D Ti–O lattice of $Na_{0.25}TiO_2$. We obtain a Ti_4O_{12} quadruple chain **3** by first sharing the edges of two Ti_2O_8 double chains, a

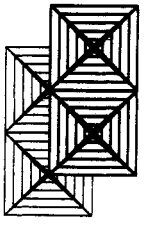

3

Ti_8O_{20} layer **4** by sharing the edges of Ti_4O_{12} quadruple chains,

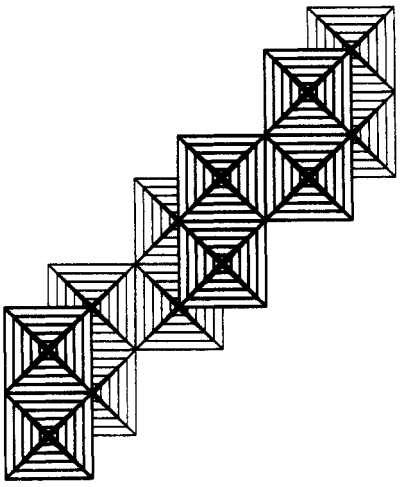

4

and finally the 3D Ti_8O_{16} lattice **5** by sharing the corners of Ti_8O_{20}

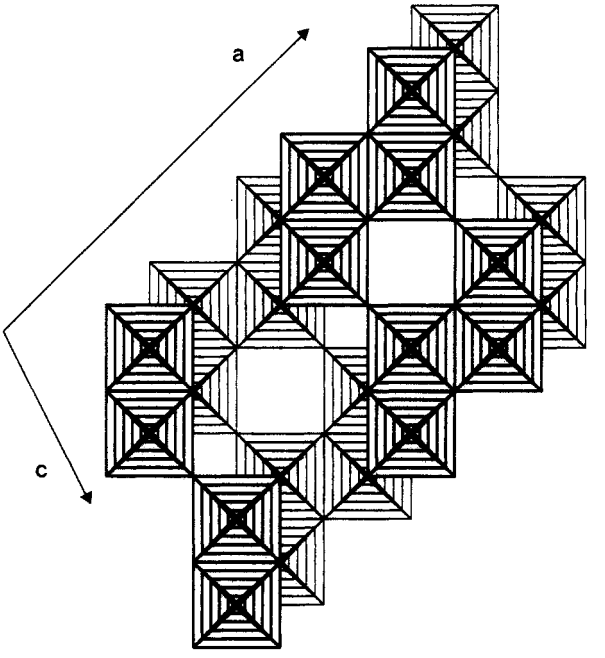

5

layers. It is in the channels between Ti_8O_{20} layers where Na atoms are located.

There are two crystallographically different Ti atoms [i.e., Ti(1) and Ti(2)] in $Na_{0.25}TiO_2$,[1a] and their TiO_6 octahedra are distorted from a regular octahedron as shown in **6**. In the Ti(1)O_6 octa-

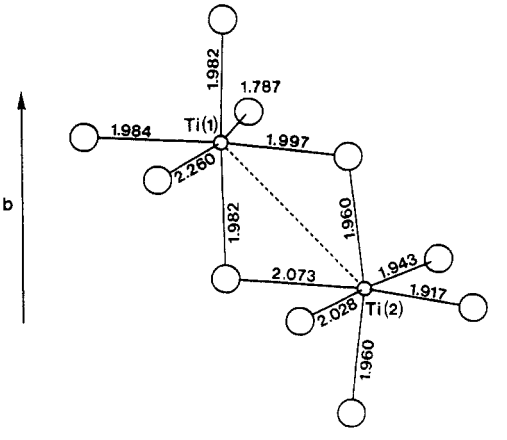

6

(6) (a) Whangbo, M.-H.; Canadell, E. *Acc. Chem. Res.* **1989**, *22*, 375. (b) Whangbo, M.-H.; Evain, M.; Canadell, E.; Ganne, M. *Inorg. Chem.* **1989**, *28*, 267.
(7) (a) Whangbo, M.-H.; Hoffmann, R. *J. Am. Chem. Soc.* **1978**, *100*, 6093. (b) Whangbo, M.-H.; Hoffmann, R.; Woodward, R. B. *Proc. R. Soc. London, A* **1979**, *366*, 23.
(8) Hoffmann, R. *J. Chem. Phys.* **1963**, *39*, 1397.
(9) (a) Whangbo, M.-H.; Canadell, E. *J. Am. Chem. Soc.* **1988**, *110*, 358. (b) Onoda, M.; Toriumi, K.; Matsuda, Y.; Sato, M. *J. Solid State Chem.* **1987**, *66*, 163.
(10) Ammeter, J. H.; Bürgi, H.-B.; Thibeault, J. C.; Hoffmann, R. *J. Am. Chem. Soc.* **1978**, *100*, 3686.

hedron, a strong O–Ti···O bond alternation (i.e., 1.787 vs 2.260 Å) exists along the direction perpendicular to the crystallographic b axis (i.e., the chain direction), and the remaining four Ti–O bonds have a similar length (approximately 1.986 Å on average). The $Ti(2)O_6$ octahedron has two long and four short Ti–O bonds, and the latter four are shorter on average (i.e., 1.945 Å) than the four intermediate Ti–O bonds of the $Ti(1)O_6$ octahedron (i.e., 1.986 Å). In the Ti_4O_{12} quadruple chain **3**, Ti(1) and Ti(2) atoms are found in the middle two and in the outer two TiO_5 chains, respectively. Consequently, $Ti(1)O_6$ octahedra form $Ti(1)_2O_8$ double chains, and these double chains are separated from one another as shown in **7**. This aspect, along with the distortions

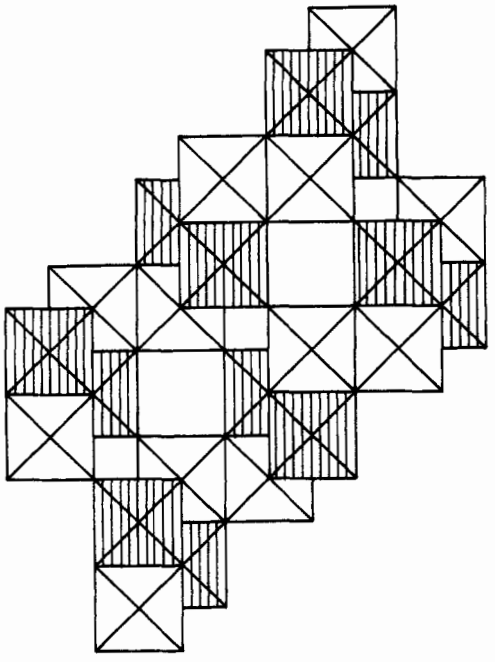

7

of the $Ti(1)O_6$ and $Ti(2)O_6$ octahedra, has an important consequence on the electronic structure of $Na_{0.25}TiO_2$.

Band Electronic Structure

Given the oxidation states of Ti^{4+} and O^{2-}, the t_{2g}-block bands of $Na_{0.25}TiO_2$ are filled due to the electrons donated by Na. The amount of donated electrons from Na is not large, i.e., one electron per four Ti atoms or, equivalently, one electron per twelve t_{2g}-block levels. Therefore, in $Na_{0.25}TiO_2$, only the bottom of the t_{2g}-block bands becomes occupied. Parts a and b of Figure 1 show the t_{2g}-block bands calculated for the Ti_2O_8 [i.e., $Ti(1)Ti(2)O_8$] double chain and the Ti_4O_{12} [i.e., $Ti(1)_2Ti(2)_2O_{12}$] chain, respectively. In both parts, the bottom bands are largely represented by the $Ti(1)O_6$ octahedra. This is due to the different types of distortion the $Ti(1)O_6$ and $Ti(2)O_6$ octahedra have, as described in the previous section. $Ti(1)O_6$ underwent a distortion that leads to one short Ti–O bond (**8a**) thereby splitting the t_{2g}-levels into one

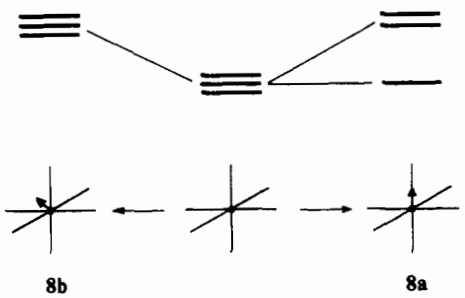

8b **8a**

δ- and two π-type orbitals with respect to the shortened Ti–O bond axis.[6] The δ orbital is not affected in energy by the distortion, but the two π orbitals are raised due to increased antibonding in the shortened Ti–O bond.[6] $Ti(2)O_6$ has a distortion that shortens

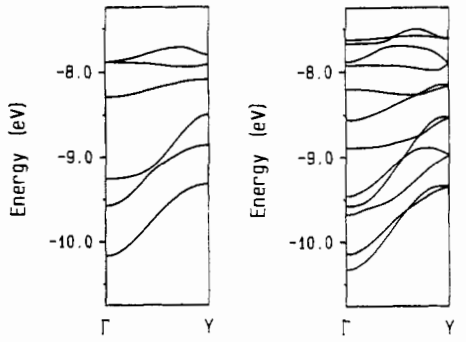

Figure 1. Dispersion relations of the t_{2g}-block bands calculated for the (a, left) Ti_2O_8 double chain **2** and the (b, right) Ti_4O_{12} quadruple chain **3**.

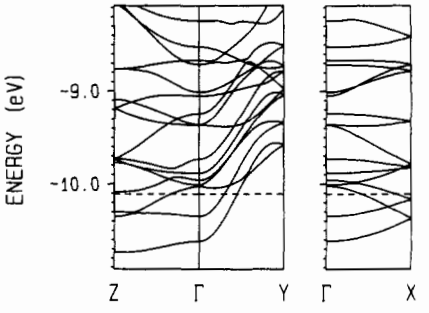

Figure 2. Dispersion relations of the bottom t_{2g}-block bands calculated for the $Ti_8O_{16}^{2-}$ lattice **5**, where the dashed line refers to the Fermi level. $\Gamma = (0, 0, 0)$, $X = (a^*/2, 0, 0)$, $Y = (0, b^*/2, 0)$, and $Z = (0, 0, c^*/2)$.

more than one Ti–O bond (**8b**), so that all its t_{2g} levels are raised in energy.[6] Consequently, the lowest lying t_{2g}-block levels come from $Ti(1)O_6$ octahedra, which explains why the bottom t_{2g}-block bands of the Ti_2O_8 and Ti_4O_{12} chains are largely represented by the lowest lying t_{2g}-block levels of $Ti(1)O_6$ octahedra. Note that, in each $Ti(1)O_6$ octahedron, the shortened Ti–O bond is oriented perpendicular to the chain axis (**6**), so that the lowest lying t_{2g}-block level has a π-type symmetry along the chain direction (i.e., the b axis) as illustrated in **9** with a $Ti(1)O_5$ chain.

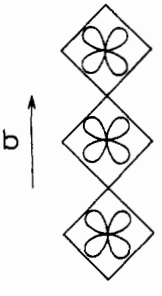

9

Figure 2 shows the bottom portion of the t_{2g}-block bands calculated for the 3D $Ti_8O_{16}^{2-}$ lattice, where the dashed line refers to the Fermi level. With only two electrons to fill them, the bottom two folded bands become partially filled. These bands are largely represented by the lowest lying t_{2g} levels of $Ti(1)O_6$ octahedra and are dispersive along the chain direction $\Gamma \rightarrow Y$, as expected from our discussion of Figure 1. The two partially filled bands are less dispersive along the directions perpendicular to the chain (i.e., $\Gamma \rightarrow X$ and $\Gamma \rightarrow Z$) due to the fact that $Ti(1)_2O_8$ double chains, which hold electrons, are separated from one another as shown in **7**.

Fermi Surfaces and Nesting

The Fermi surfaces associated with the upper and lower partially filled bands of Figure 2 are shown as stereodiagrams in parts a and b of Figure 3, respectively, where a primitive reciprocal unit cell is represented by a parallelepiped. Since each band is folded in Figure 2, the Fermi surface is represented in an extended zone scheme in Figure 3. The Fermi surface of the upper band (Figure

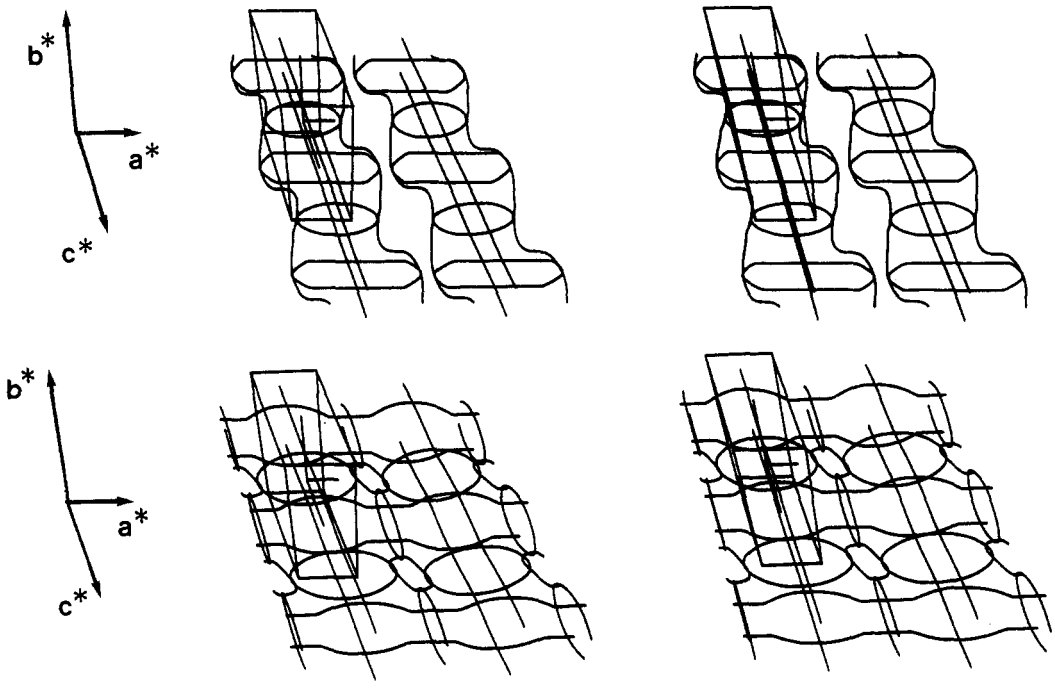

Figure 3. Stereoviews of Fermi surfaces associated with the (a, top) upper and (b, bottom) lower partially filled bands of Figure 2.

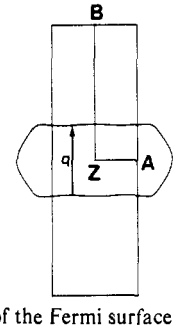

Figure 4. Cross section of the Fermi surface of Figure 3a in the vicinity of Z, where $A = (0.5a^*, 0, 0.5c^*)$, $B = (0, 0.5b^*, 0.5c^*)$, and $q \approx 0.25b^*$.

3a) has a shape of a zigzagging tunnel running along the c^* direction and flattened along the b^* direction. The Fermi surface of the lower band (Figure 3b) has the shape of cross-linked tunnels running along the a^* and c^* directions. If the two partially filled bands of Figure 2 were perfectly 1D in nature (i.e., no dispersion along $\Gamma \rightarrow X$ and $\Gamma \rightarrow Z$ directions), the resulting Fermi surface of each band would be given by two parallel planes perpendicular to the b^* axis. The Fermi surfaces of Figure 3a,b deviate from this ideal shape because of nonvanishing interactions among the $Ti(2)O_8$ chains through the $Ti(2)O_6$ octahedra and hence do not exhibit a perfect nesting. Nevertheless, the Fermi surface of the upper band (Figure 3a) is flatter than that of the lower band (Figure 3b) and, consequently, shows a partial nesting along the b^* direction [especially in the vicinity of the wave vector point $Z = (0, 0, 0.5c^*)$] as shown in Figure 4, where $q \approx 0.25b^*$.

The presence of CDW superlattice spots in $Na_{0.25}TiO_2$ with a q_{b^*} component of $0.230 - 0.245b^*$ shows that $Na_{0.25}TiO_2$ is more 1D in character than is predicted by the present band electronic structure study. It is possible that our calculation might have overemphasized interchain interactions or that the crystal structure of $Na_{0.25}TiO_2$ determined at room temperature is not quite accurate since it neglected the superlattice reflections in the structural refinement. Nevertheless, it is quite clear from our study that $Na_{0.25}TiO_2$ is essentially a 1D-like metal. In addition, Figure 2 shows that the bottom of a third band lies above, but very close to, the Fermi level. Consequently, thermal excitation of electrons into this band, as dictated by the Fermi–Dirac distribution law, will leave less than two electron for the bottom two bands thereby leading to a smaller q_{b^*} value. When the temperature is lowered, the extent of this thermal excitation would decrease, thereby increasing the q_{b^*} value, as in the case of blue bronze $A_{0.3}MoO_3$.[3a,5]

Concluding Remarks

Although $Na_{0.25}TiO_2$ has a complex 3D Ti–O lattice made up of TiO_6 octahedra, its electronic structure is 1D as evidenced by the observation of CDW superlattice reflections. This results from the fact that there exist two nonequivalent TiO_6 octahedra, i.e., $Ti(1)O_6$ and $Ti(2)O_6$, which differ in their distortions. $Ti(1)O_6$ octahedron provides the lowest lying t_{2g}-block level, and $Ti(1)_2O_8$ double chains are separated from one another by $Ti(2)O_6$ octahedra in $Na_{0.25}TiO_2$. Consequently, $Na_{0.25}TiO_2$ is 1D electronically despite its 3D crystal lattice. This situation is quite similar to lithium molybdenum purple bronze $Li_{0.9}Mo_6O_{17}$. The temperature dependence of the CDW vector q_{b^*} in $Na_{0.25}TiO_2$ originates from the fact that $Na_{0.25}TiO_2$ has an empty band whose bottom lies very close to the Fermi level. A similar phenomenon has been observed for the blue bronze $A_{0.3}MoO_3$.[3a,5]

Acknowledgment. This work was supported by the U.S. Department of Energy, Office of Basic Energy Sciences, Division of Materials Sciences, under Grant DE-FG-05-86ER45259. We express our appreciation for computing time on the ER-Cray X-MP computer made available by DOE.